P2.11 THE IMPACT OF EVAPORATION ON POLARIMETRIC CHARACTERISTICS OF RAIN: THEORETICAL MODEL AND PRACTICAL IMPLICATIONS

MATTHEW R. KUMJIAN AND ALEXANDER V. RYZHKOV
CIMMS, University of Oklahoma, and NOAA/OAR National Severe Storms Laboratory, Norman, Oklahoma, USA

1. INTRODUCTION

With the upgrade of the National Weather Service WSR-88D radar network to dual-polarization capabilities comes additional information that operational meteorologists can use to better diagnose and predict the local weather (e.g., Zrnić and Ryzhkov 1999; Ryzhkov et al. 2005a). Because polarimetric radars are quite sensitive to certain phenomena including hydrometeor phase transitions and size sorting, it is important to understand how such microphysical processes impact the measured polarimetric variables. For example, the important polarimetric "bright band" signature associated with melting graupel and snow is well documented (e.g., Brandes and Ikeda 2004; Giangrande et al. 2005, 2008). Additionally, polarimetric observations of size sorting can reveal important information about storm kinematics, including the low-level storm-relative helicity in supercell environments (Kumjian and Ryzhkov 2009).

In contrast, the impact of evaporation on polarimetric observables has received comparatively little attention. Understanding and quantifying evaporation is of significant importance in the field of hydrology for quantitative precipitation estimation. Despite the many studies that quantify the impact of environmental conditions on the rate of evaporation and how evaporation affects the rainfall rate, drop size distribution, and radar reflectivity factor (e.g., Srivastava 1985, 1987; Rosenfeld and Mintz 1988; Hu and Srivastava 1995), there is a paucity of studies investigating how varying evaporation rates are manifest in the polarimetric variables. A notable exception is Li and Srivastava (2001), who quantified the impact of evaporation on the differential reflectivity Z_{DR}. In contrast, the purpose of this paper is to quantify the sensitivity of all the polarimetric variables to various environmental thermodynamic conditions, variations in drop size distributions (DSDs), and rainfall rates, as well as to formulate recommendations to aid in hydrometeorological rainfall estimation.

Corresponding Author Address: Matthew R. Kumjian, 120 David L. Boren Blvd., National Weather Center Suite 4900, Norman, OK 73072. E-mail: matthew.kumjian@noaa.gov

2. BACKGROUND

Following the nationwide upgrade of the WSR-88D radar network, meteorologists will have for their use a full slate of polarimetric variables in addition to the conventional radar reflectivity factor at horizontal polarization (Z_H) and Doppler velocity (v_r). These additional variables are differential reflectivity (Z_{DR}), differential phase (Φ_{DP}) and specific differential phase (K_{DP}), and the copolar cross-correlation coefficient at zero lag (ρ_{HV}). The reader is directed to descriptions of these variables in the literature (e.g., Herzegh and Jameson 1992; Doviak and Zrnić 1993; Zrnić and Ryzhkov 1999; Straka et al. 2000; Ryzhkov et al. 2005a).

Liquid drops in clouds can grow by the diffusion of water vapor from the ambient environment if the ambient vapor density is greater than the vapor density at the droplet's surface. On the other hand, if the vapor density at the surface of the drop exceeds the vapor density in the ambient environment, vapor is diffused away from the drop (evaporation). The rate of mass diffusion can be written as

$$\frac{dm}{dt} = 4\pi r D_v\left(\rho_v - \rho_{vr}\right) \tag{1}$$

where r is the radius of the drop, D_v is the molecular diffusion coefficient, and ρ_v and ρ_{vr} are the vapor density of the ambient environment and at the surface of the drop, respectively. Following Pruppacher and Klett (1978) and Rogers and Yau (1989), one can derive an approximate expression describing the rate of change of the drop radius

$$r\frac{dr}{dt} = \frac{S-1}{F_K + F_D} \tag{2}$$

where S is the saturation ratio, and F_K and F_D are terms related to heat conduction and vapor diffusion, respectively; their functional dependence on environmental conditions can be found in Rogers and Yao (1989), Pruppacher and Klett (1978), or in the full version of this study (Kumjian and Ryzhkov 2010). For now, we simply focus on a qualitative interpretation of (2). For subsaturated environments (where $S < 1$), drop radius will decrease, indicating decay through evaporation. Also note that dr/dt is inversely proportional to the radius of the drop, meaning that smaller drops will undergo more rapid evaporation than larger drops. This well-known fact is important when considering the impact of evaporation on polarimetric variables.

Theoretically, the preferential depletion of smaller drops will result in a decrease in observed Z_H and K_{DP} with an increase in the observed Z_{DR}. The observed

decrease in Z_H has been well documented and is intuitive. Decreasing drop diameters across the spectrum and a decrease in the concentration of smaller drops (those that are totally evaporated) will result in a decreased magnitude of backscattered signal. Recall that K_{DP} is less sensitive than Z_H to large drops, and as a corollary, more sensitive to changes in the lower end of the drop size spectrum. Therefore, one can expect evaporation to affect K_{DP} more substantially than Z_H.

The expected increase in Z_{DR} is less intuitive because all drops are losing mass (size). However, since Z_{DR} is a measure of the median drop size in a distribution, a preferential depletion of smaller drops which generally have a large concentration causes an increase in the median drop size of a given DSD. This effect is shown schematically in Fig. 1. At S band, the change in ρ_{HV} due to evaporation in pure rain is not expected to be significant for reasons discussed in a later section. The magnitude of changes in all polarimetric variables should be dependent on the relative contributions of small drops and large drops and thus is strongly dependent on the DSD.

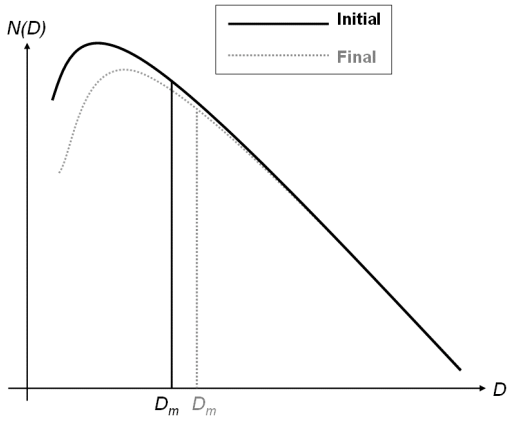

Fig. 1: Conceptual schematic illustrating how evaporation can cause an increase in the median drop size D_m of a distribution. The solid black lines indicate the DSD before evaporation occurs; the dashed gray lines represent the modified DSD due to evaporation.

3. MODEL

3.1. Description

In an effort to quantify the impact of evaporation on the polarimetric variables under different conditions and assumptions, a simple numerical model is constructed. The idealized one-dimensional model explicitly computes the change in size of raindrops falling through subsaturated air. The model domain is the subcloud layer, and 100-m vertical resolution is used in this study. Eighty initial drop sizes are considered, ranging from 0.05 mm to 7.95 mm in 0.1-mm increments. Each drop size "bin" is tracked independently in order to isolate the effects of evaporation. Hence, no drop interactions such as collisions, coalescence, or breakup are taken into account. Note that coalescence and breakup significantly contribute to the evolution of the drop size spectrum, as found in numerous theoretical and modeling studies (Low and List 1982; Brown 1986, 1987; Seifert et al. 2005; Seifert 2008). These collisional processes become increasingly important in heavier rainfall. On the other hand, evaporation tends to only change the slope of the DSD slowly, instead mainly affecting the total water content (e.g., Srivastava 1978). For rainfall estimation, evaporation is most important since it is the only subloud process that directly affects the total mass of rain water reaching the ground. The relative contributions to depletion of total water content from combinations of coalescence, breakup, and evaporation have been investigated previously (e.g., Hu and Srivastava 1995; Seifert 2008). Hu and Srivastava (1995) found that the effects of coalescence and breakup tend to approximately balance. In their model, total rainwater mass depletion in simulations that employed full microphysics (coalescence, breakup and evaporation) was similar to those in which only evaporation was considered. Thus, only including evaporation in this model, although inherently limiting its applicability towards simulating the evolution of the DSD, is justifiable to improve computational efficiency of the model given our focus on the radar measurements and associated rainfall estimation.

At the top of the domain, or in the "cloud," any drop size distribution model can be prescribed. In the sub-cloud domain, any vertical profile of temperature and relative humidity can be administered. In our shaft model, the feedback on the environmental thermodynamic profiles due to evaporation may be turned on or off. For simplicity, the feedback will be turned off in this study. In reality, the shaft will gradually moisten and cool due to evaporation of raindrops into the subsaturated air, thereby decreasing the impact of evaporation with time. As such, the evaporation may be too aggressive in our model. Since the model is one-dimensional, no size sorting due to vertical shear (e.g., Kumjian and Ryzhkov 2009) is considered. At the initial time, the drops begin to fall into the top of the domain, as in many rainshaft models. After numerous tests, the time step was selected to be 0.25 seconds, maximizing computational efficiency while maintaining stable solutions. Since the model is fully time dependent, the transient differential sedimentation size sorting effect is captured.

3.2. Equations

We are interested in the vertical profiles of the polarimetric variables, so we convert (2) into an expression for the change in drop radius with height by dividing (2) by the fall speed of raindrops as a function of

size. To simplify the ensuing integration, the empirical power law fall speed relation suggested by Atlas and Ulbrich (1977) is used for the terminal velocity of the raindrops

$$v_t(D) = \alpha D^{\beta}\left(\frac{\rho_0}{\rho_a}\right)^{0.4} \quad (3)$$

where α = 3.78 m s^{-1} mm$^{-0.67}$, β = 0.67, and the equivalent spherical diameter D is given in mm. The multiplicative factor $\left(\rho_0/\rho_a\right)^{0.4}$ is a density correction, where ρ_0 is the surface reference density value following Foote and duToit (1969). Though (3) is less accurate for large drops than more recent empirical models (e.g., Brandes et al. 2002), it well represents the fall speeds of smaller drops (< 5 mm) for which evaporation effects are most significant. Thus, performing the change of variables in equation (2) and using the velocity relation (3) yields an analytic expression for the change in diameter of a raindrop with initial size D_0 as a function of height

$$D(h) = \left[D_0^{\beta+2} + \frac{4(\beta+2)}{\alpha}\int_{h_0}^{h}\xi(h')\left(\frac{\rho_a(h')}{\rho_0}\right)^{0.4} dh'\right]^{\frac{1}{\beta+2}} \quad (4)$$

where we have defined ξ as the right hand side of equation (2). To numerically integrate this expression, ξ and ρ_a are assumed to be constant over each height step $\Delta h = h_i - h_{i+1}$, which should be relatively small (100 m is used in this study), resulting in

$$D(h_{i+1}) = \left[D(h_i)^{\beta+2} + \frac{4\xi(\beta+2)}{\alpha}\left(\frac{\rho_a}{\rho_0}\right)^{0.4}\Delta h\right]^{\frac{1}{\beta+2}} \quad (5)$$

In this way, the simple expression (5) is used to create look-up tables for what a given initial drop size should be at any height beneath the cloud base for given thermodynamic profiles and assuming the drops are falling at terminal velocity.

The mass concentration of raindrops $n(m)$ in many of the aforementioned modeling studies is governed by the following equation

$$\frac{\partial}{\partial t}\left[n(m)\right] + \frac{\partial}{\partial z}\left[v_t n(m)\right] + \frac{\partial}{\partial m}\left[\dot{m} n(m)\right] = 0 \quad (6)$$

where the second term on the left hand side is the change in drop concentration due to differential sedimentation, where v_t is the drop terminal fall speed, and where the collisional effects of coalescence and breakup have been left off. The third term describes the change in concentration of drops of mass m due to growth or decay by vapor diffusion, i.e., condensation or evaporation. For the calculation of radar variables, it is more convenient to have the drop concentration in terms of diameter D. Thus, we seek an expression of (6) in terms of $N(D)$, where $N(D)dD$ is the number of raindrops of size D to $D + dD$. The concentrations $n(m)$ and $N(D)$ are related by

$$n(m) = N(D)\frac{dD}{dm} \quad (7)$$

Assuming spherical symmetry of the raindrops, $m = (\pi/6)\rho_l D^3$, where ρ_l is the density of liquid water. Thus, substituting (7) into (6), evaluating dD/dm, rewriting the mass diffusion in terms of D, and making use of the change of variables

$$\frac{\partial}{\partial m} = \frac{dD}{dm}\frac{\partial}{\partial D}$$

Yields the governing equation in terms of drop diameter D:

$$\frac{\partial}{\partial t}\left[N(D)D^{-2}\right] = -\frac{\partial}{\partial z}\left[v_t n(D)D^{-2}\right] - \frac{1}{D^2}\frac{\partial}{\partial D}\left[\dot{D}N(D)\right] \quad (8)$$

The change in diameter of the drop size bins at each height level and the drop concentration at each level are used to compute the vertical profiles of polarimetric variables according to the T-Matrix method (e.g., Mishchenko 2000). The raindrops are assumed to have a distribution of canting angles with mean 0° and standard deviation 20° with respect to the vertical. The wavelength of the radar will be discussed using convention, according to which "S band" refers to 10.9-cm wavelength (as in the WSR-88D radar network) and "C band" refers to a wavelength of 5.3 cm. The calculations using the evaporation model will be described below and include both idealized sensitivity studies and simulations of more realistic environmental conditions.

4. CALCULATIONS

4.1. Setup

Because of the aforementioned differences in drop size dependency for each of the polarimetric variables, some degree of sensitivity to selection of the DSD is expected. To address this, each model sensitivity experiment is run several times, using different initial DSDs, including the standard exponential and gamma models,

$$N(D) = N_0 \exp\left(-\Lambda D\right) \quad (9)$$

and

$$N(D) = N_0 D^{\mu} \exp\left(-\Lambda D\right) \quad (10)$$

In order to conduct a fair comparison between the different DSD models, the surface rainfall rate (in the absence of any evaporation) for each has been fixed at 5 mm hr^{-1}. A Marshall-Palmer DSD (herein MP) is used for the exponential model, where N_0 is fixed at 8000 m^{-3} mm^{-1}. For the MP distribution, there exists a well-known relation between the slope parameter Λ and rainfall rate R:

$$\Lambda = 4.1R^{-0.21} \quad (11)$$

where R is in mm hr^{-1} and Λ is in mm^{-1}. The gamma model has three parameters, though these are usually

constrained and thus not entirely independent (e.g., Zhang et al. 2001, 2006; Brandes et al. 2004; Cao et al. 2008). For Oklahoma precipitation, Cao et al. (2008) found empirically that the shape parameter μ and the slope parameter Λ are related by

$$\mu = -0.0201\Lambda^2 + 0.902\Lambda - 1.718 \qquad (12)$$

where the equation is applicable for Λ values between 0 and 20. For this study, constrained gamma models with μ varying between -1 and 5 in increments of one are used in the calculations. These values encompass the bulk of observations in Oklahoma rain. Fig. 2 presents the different modeled DSDs. It is evident that a variety of DSD shapes have been selected for this study, covering a broad spectrum of precipitation regimes.

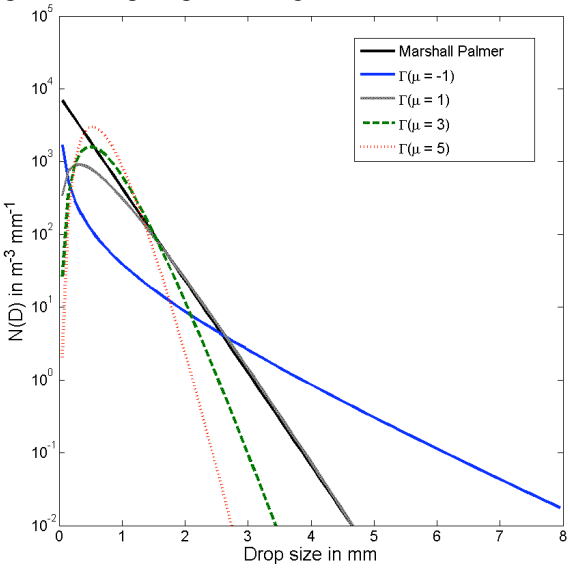

Fig. 2: DSD models used for the simulations: The Marshall-Palmer (solid black line), μ = -1 gamma model (Γ,μ=-1; solid blue line), the μ = +1 gamma model (Γ,μ=1; solid gray line), the gamma model with μ = +3 (Γ,μ=3; dashed green line), and the gamma model with μ = +5 (Γ,μ=5; dotted red line). All models are for rainfall rates of 5 mm hr^{-1}.

In the first set of sensitivity tests, an isothermal layer of 2km in depth with a temperature of 20 °C is used. The relative humidity profiles are set constant in height and vary from 10% to 95%. Next, simulations of well-mixed boundary layers are performed. The domain is 3 km in depth with a surface temperature of 30 °C in each case, while surface humidity varies from 60%-90% and in each case increases linearly to 100% at the top of the domain (i.e., at the cloud). Finally, we use observed soundings to simulate real environments. For brevity, one such sounding-based simulation will be shown in this paper (Fig. 3).

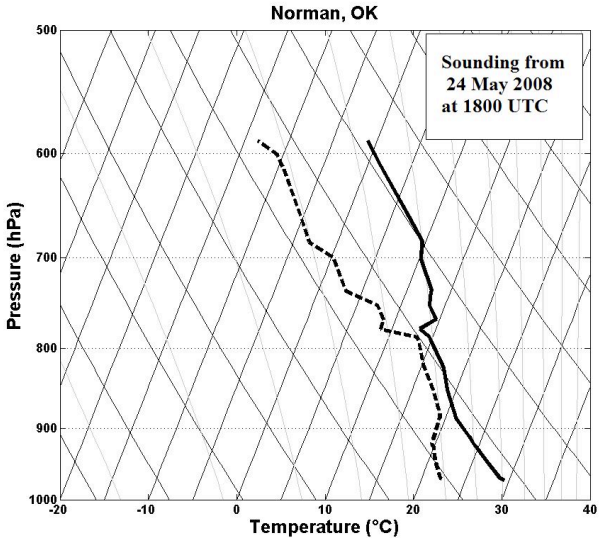

Fig. 3: Sounding from Norman, OK (OUN) taken at 1800 UTC on 24 May 2008. This sounding is used in the model simulations.

4.2. Results

At the onset of precipitation from a cloud, there is a transient effect known as differential sedimentation. In this form of size sorting, the larger drops fall out faster than the smaller drops. Since polarimetric radar measurements (especially Z_{DR}) are strongly sensitive to size sorting, the initial effect of differential sedimentation dominates the calculated variables. Thus, the effect of evaporation on the polarimetric variables is negligible in comparison to differential sedimentation while this transient effect is occurring, which is manifest as a sharp drop off in Z_H and K_{DP} and a substantial increase in Z_{DR} towards the ground. At S band, ρ_{HV} does not change drastically, though at C band there is a considerable drop in ρ_{HV} at the leading edge of the large drops due to resonance scattering effects characteristic of those drop sizes (Fig. 4). After long enough time has lapsed such that all drop sizes have reached all levels beneath the cloud, differential sedimentation is no longer an issue and the effects of evaporation are isolated from those of this initial size sorting. We shall consider the rainshaft to be in a steady state at this point in time.

The results of the isothermal layer sensitivity tests are displayed in Figs. 5-6 (at S and C bands, respectively). It is clear that all of the variables are sensitive to changes in relative humidity (given a constant temperature), but perhaps more importantly the results are sensitive to the initial DSD model selected. The Γ,μ=5 model exhibits much greater evaporative change in Z_H than the other models (Figs. 5a, 6a). This is explained by two factors. First, the distribution contains a large concentration of small drops, which are preferentially evaporated, resulting

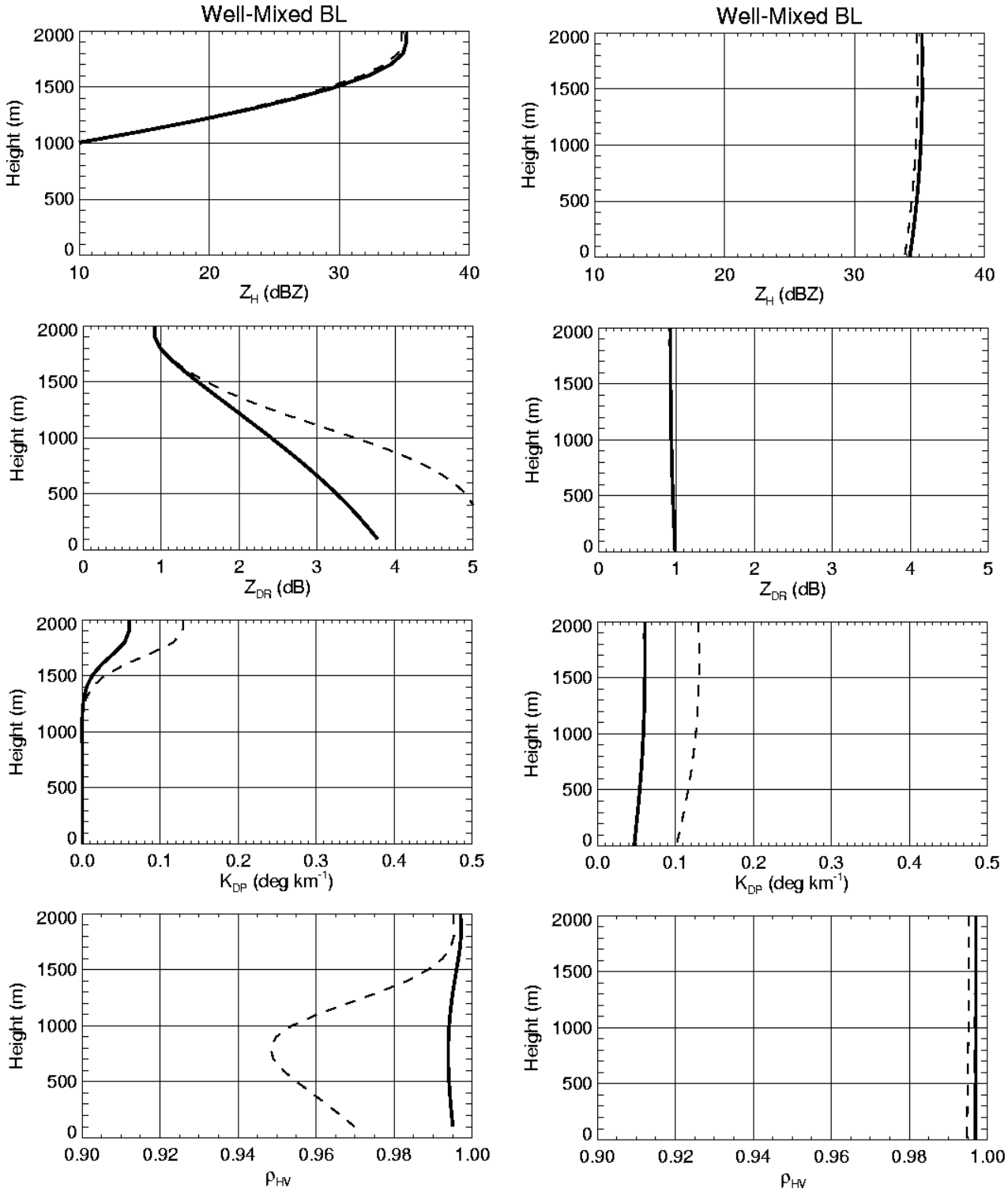

Fig. 4: Example of transient differential sedimentation 60 seconds into a model run the MP DSD falling into a well-mixed boundary layer with surface relative humidity of 70% (left column). The right column shows the same simulation after a steady state has been achieved. The solid lines indicate S-band values, and the dashed lines indicate C-band values.

in a substantial decrease in mass. Second, the Γ,μ=5 has fewer large drops than any other distribution. These large drops (which do not evaporate as efficiently as smaller drops) tend to overwhelm the contribution to the observed Z_H (and to a lesser extent, K_{DP}) for the other DSD models, which all exhibit lower magnitudes of ΔZ_H.

The results of the isothermal layer sensitivity tests are displayed in Figs. 5-6 (at S and C bands, respectively). It is clear that all of the variables are sensitive to changes in relative humidity (given a constant temperature), but perhaps more importantly the results are sensitive to the initial DSD model selected. The Γ,μ=5 model exhibits much greater evaporative change in Z_H than the other models (Figs. 5a, 6a). This is explained by two factors. First, the distribution contains a large concentration of small drops, which are preferentially evaporated, resulting in a substantial decrease in mass. Second, the Γ,μ=5 has fewer large drops than any other distribution. These large drops (which do not evaporate as efficiently as smaller drops) tend to overwhelm the contribution to the observed Z_H (and to a lesser extent, K_{DP}) for the other DSD models, which all exhibit lower magnitudes of ΔZ_H.

Since Z_{DR} is more sensitive to drop size than Z_H, it follows that the large ΔZ_{DR} values occur for the DSDs with large concentrations of big drops. However, also playing an important role in producing the significant ΔZ_{DR} values is a large concentration of small drops. The preferential evaporation of a significant portion of the spectrum will substantially increase the median drop size of the spectrum. This is why the MP model (which has the largest concentration of small drops and a large concentration of big drops) has the highest ΔZ_{DR} (Figs. 5b, 6b).

At S band, $\Delta\rho_{HV}$ magnitudes are quite small (< 0.01 even for extreme evaporation) for all DSD shapes, at least for the electromagnetic scattering model employed in this study (Fig. 5d). Such small changes are insignificant and likely within the uncertainty of the WSR-88D measurements. At C band, the evaporative changes in ρ_{HV} and K_{DP} are slightly larger in magnitude (Fig. 6c,d). For modest evaporation rates, changes in ρ_{HV} at both radar wavelengths are insignificant and probably difficult to detect operationally.

Using the observed sounding (Fig. 3) from Norman, each of the five DSD models is used to simulate the evaporative changes given realistic environmental conditions. Vertical profiles of the polarimetric variables are presented in Fig. 7. One can clearly see that there exists a wide variety to the resulting vertical profiles, even though the initial rainfall rate was fixed. The large variation is due entirely to the choice of DSD model aloft. Note that the DSD model with the smallest initial Z_H (the Γ,μ=5 model) ends up with the largest change in Z_H. Note that even the sign of the change in ρ_{HV} depends on the DSD choice. Figure 8 displays the calculated rainfall rates (based on each of the DSDs) as a function of height for the same Norman sounding. Here again we find a considerable variation in the resulting profiles. This underscores the uncertainty involved in quantitative precipitation estimation if the shape of the DSD is unknown.

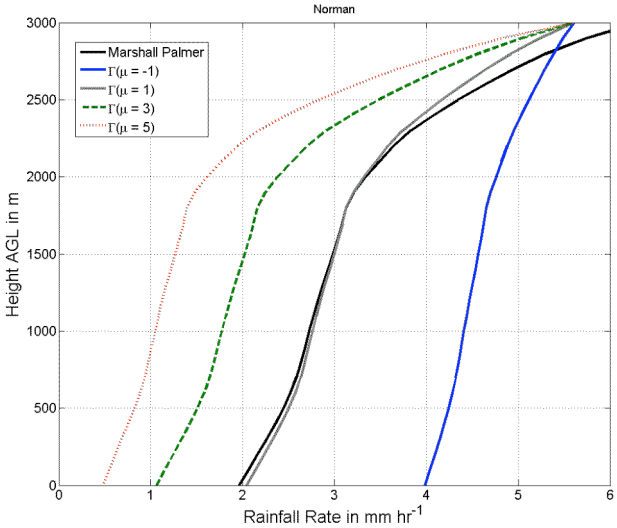

Fig. 8: As in Fig. 7, but the vertical profile of rainfall rate is plotted.

5. DISCUSSION

It is clear that DSD variability aloft creates considerable uncertainty. When it comes to rainfall estimation, there are several relations based on polarimetric measurements suggested in the literature (see Ryzhkov et al. 2005c; Giangrande and Ryzhkov 2008). When applying these relations to the model output for numerous simulations, it was found that the most accurate relation is different for differerent initial DSD choices. The difficulty for operational forecasters is to determine the initial DSD aloft. There are rigorous methods for DSD retrieval based on polarimetric radar measurements, such as the procedures described in Zhang et al. (2001, 2006), and Brandes et al. (2002, 2004). These methods mainly rely on Z_H and Z_{DR} measurements.

We now investigate the possibility of a simpler method that provides forecasters with a rough qualitative estimate of the DSD shape, upon which they can base their decisions on the relative impact of evaporation on the vertical profiles of polarimetric variables and rainfall rate. With the constrained-gamma DSD models, the *relative change in rainfall rate due to evaporation* (ΔR/R) *is independent of the initial Z_H aloft*. Thus, ΔR/R is a function of the

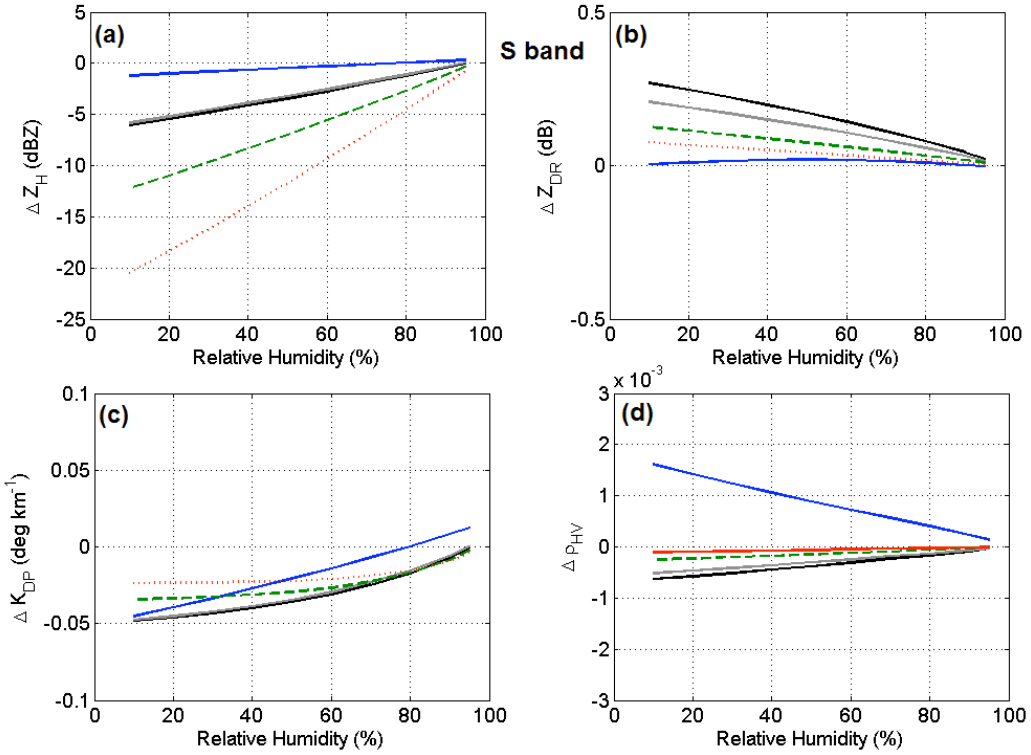

Fig. 5: Evaporative changes in the polarimetric variables at S band: (a) Z_H, (b) Z_{DR}, (c) K_{DP}, and (d) ρ_{HV}. The plotting convention is the same as that used in Fig. 2. Calculations based on a 2-km deep isothermal (20 °C) layer with constant relative humidity as indicated.

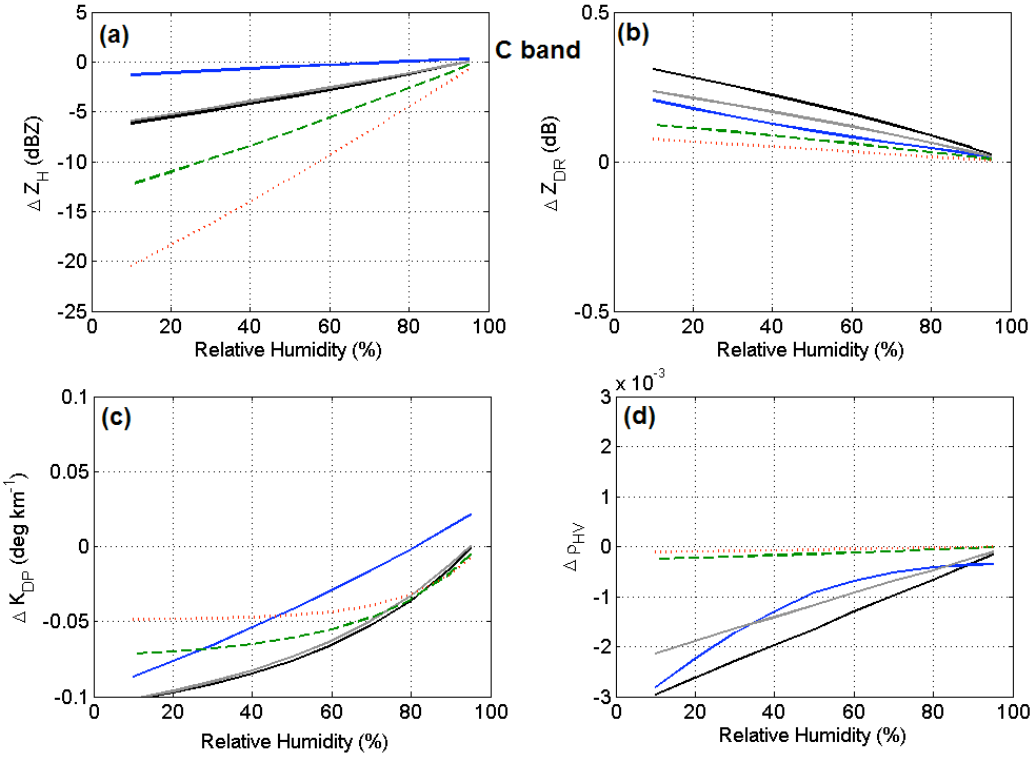

Fig. 6: As in Fig. 5, except for C band.

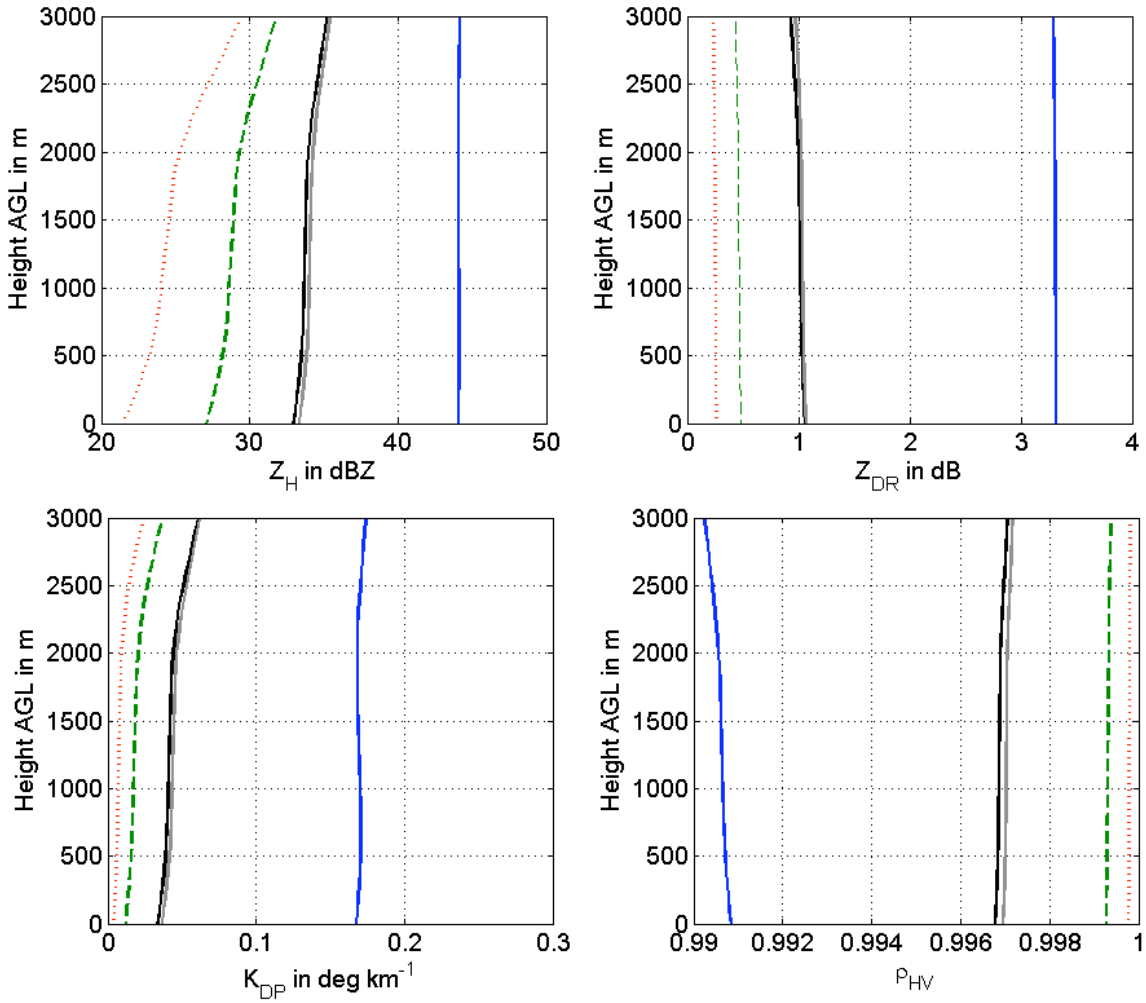

Fig. 7: Vertical profiles of the polarimetric variables resulting from a model simulation using the Norman sounding (Fig. 3). The plotting convention is the same as that used in Fig. 2.

environment (including temperature, relative humidity, and depth) and initial Z_{DR} aloft. An analysis technique based on simple modeling can be used operationally. Observations of Z_H and Z_{DR} at cloud base can be used to identify the initial rainfall rate aloft. Next, the relative humidity profile in the layer beneath the radar horizon can be determined from observations or model output. Automated algorithms can generate "look-up" tables using values of Z_{DR} aloft and relative humidity in the layer beneath the radar horizon to estimate the relative change in rainfall rate over a depth.

Forecasters can implement these automated "look-up" tables using a simple modeling approach coupled with information about the thermodynamic conditions in the region. Such information is available from soundings or even operational numerical weather prediction models. The model presented in this paper runs in a fraction of a second, so populating look-up tables is not a computationally expensive task. In this manner, the forecaster can obtain an estimate of the amount of rainfall reaching the surface when the radar cannot adequately scan at low levels, aiding improving quantitative precipitation estimation. Such improved rainfall estimates are of critical importance in operational hydrology and meteorology.

6. REFERENCES

Atlas, D. and C.W. Ulbrich, 1977: Path- and area-integrated rainfall measurement by microwave attenuation in the 1 – 3 cm band. *J. Appl. Meteor.*, **16**, 1322-1331.

Brandes, E.A. and K. Ikeda, 2004: Freezing-level estimation with polarimetric radar. *J. Appl. Meteor.*, **43**, 1541-1553.

Brandes, E.A., G. Zhang, and J. Vivekanandan, 2002: Experiments in rainfall estimation with a polarimetric radar in a subtropical environment. *J. Appl. Meteor.*, **41**, 674-685.

Brandes, E.A., G. Zhang, and J. Vivekanandan, 2004: Drop size distribution retrieval with polarimetric radar: Model and application. , **43**, 461–475.

Brown, P.S., 1986: Analysis of the Low and List drop-breakup formulation. *J. Climate Appl. Meteor.*, **25**, 313-321.

−−−−, 1987: Parameterization of drop-spectrum evolution due to coalescence and breakup. *J. Atmos. Sci.*, **44,** 242-249.

Cao, Q., G. Zhang, E. Brandes, T. Schuur, A.V. Ryzhkov, and K. Ikeda, 2008: Analysis of video disdrometer and polarimetric radar data to characterize rain microphysics in Oklahoma. *J. Appl. Meteor. and Climatology*, **47**, 2238-2255.

Doviak, R.J. and D.S. Zrnić, 1993: *Doppler Radar and Weather Observations*. Academic Press, 562 pp.

Foote, G.B., and P.S. duToit, 1969: Terminal velocity of raindrops aloft. *J. Appl. Meteorology*, **8**, 249-253.

Giangrande, S.E., J.M. Krause, and A.V. Ryzhkov, 2008: Automatic designation of the melting layer with a polarimetric prototype of the WSR-88D radar. *J. Appl. Meteor. and Climatology,* **47**, 1354-1364**.**

−−−− and A.V. Ryzhkov, 2008: Estimation of rainfall based on the results of polarimetric echo classification. *J. Appl. Meteor. and Climatol.*, **47**, 2445-2462.

−−−−, A. V. Ryzhkov, and J. Krause, 2005: Automatic detection of the melting layer with a polarimetric prototype of the WSR-88D radar. Extended Abstracts, *32nd Int. Conf. on Radar Meteorology*, Albuquerque, NM, USA, Amer. Meteor. Soc., CD-ROM, 11R.2.

Herzegh, P.H. and A.R. Jameson, 1992: Observing precipitation through dual-polarization radar measurements. *Bull. Amer. Meteor. Soc.*, **73**, 1365-1374.

Hu, Z., and R. Srivastava, 1995: Evolution of raindrop size distribution by coalescence, breakup, and evaporation: Theory and observations. *J. Atmos. Sci.*, **52**, 1761–1783.

Kumjian, M.R. and A.V. Ryzhkov, 2009: Storm-relative helicity revealed from polarimetric radar measurements. *J. Atmos. Sci.*, **66**, 667-685.

Li, X., and R.C. Srivastava, 2001: An analytical solution for raindrop evaporation and its application to radar rainfall measurements. *J. Appl. Meteor.*, **40**, 1607–1616.

Low, T.B. and R. List, 1982: Collision, coalescence, and breakup of raindrops. Part II: Parameterization of fragment size distributions. *J. Atmos. Sci.*, **39**, 1607-1618.

Mishchenko, M.I. 2000: Calculation of the amplitude matrix for a nonspherical particle in a fixed orientation. *Appl. Optics*, **39**, 1026-1031.

Pruppacher, H.R. and J.D. Klett, 1978: *Microphysics of Clouds and Precipitation*, 2nd ed. Oxford University Press, 953 pp.

Rogers, R.R. and M.K. Yau, 1989: *A Short Course in Cloud Physics*, 3rd ed. Elsevier Press, 290 pp.

Rosenfeld, D. and Y. Mintz, 1988: Evaporation of rain falling from convective clouds as derived from radar measurements. *J. Appl. Meteor.*, **27**, 209-215.

Ryzhkov, A.V., T.J. Schuur, D.W. Burgess, P.L. Heinselman, S.E. Giangrande, and D.S. Zrnić, 2005a: The joint polarization experiment. *Bull. Amer. Meteor. Soc.*, **86**, 809-824.

−−−−, S.E. Giangrande, and T.J. Schuur, 2005b: Rainfall estimation with a polarimetric prototype of WSR-88D. *J. Appl. Meteor.*, **44**, 502-515.

Seifert, A., 2008: On the parameterization of evaporation of raindrops as simulated by a one-dimensional rainshaft model. *J. Atmos. Sci.*, **65**, 3608-3619.

−−−−, A. Khain, U. Blahak, and K.D. Beheng, 2005: Possible effects of collisional breakup on mixed-phase deep convection simulated by a spectral (bin) cloud model. *J. Atmos.Sci.*, **62**, 1917-1931.

Srivastava, R.C., 1978: Parameterization of raindrop size distributions. *J. Atmos. Sci.*, **35**, 108-117.

−−−−, 1985: A simple model of evaporatively driven dowadraft: Application to microburst downdraft. *J. Atmos. Sci.*, **42**, 1004–1023.

−−−−, 1987: A model of intense downdrafts driven by the melting and evaporation of precipitation. *J. Atmos. Sci.*, **44**, 1752–1774.

Straka, J.M., D.S. Zrnić, and A.V. Ryzhkov, 2000: Bulk hydrometeor classification and quantification using polarimetric radar data: synthesis of relations. *J Appl. Meteor.*, **39**, 1341-1372.

Zhang, G., J. Sun, and E.A. Brandes, 2006: Improving parameterization of rain microphysics with disdrometer and radar observations. *J. Atmos. Sci.*, **63**, 1273–1290.

−−−−, J. Vivekanandan, and E. Brandes, 2001: A method for estimating rain rate and drop size distribution from polarimetric radar measurements. *IEEE Trans. Geosci. Remote Sens.,* **39,** 830–841.

Zrnić, D.S. and A.V. Ryzhkov, 1999: Polarimetry for weather surveillance radars. *Bull. Amer. Meteor. Soc.*, **80**, 389-406.